Surface gap solitons in exciton polariton condensates

Ting-Wei Chen[1] and Szu-Cheng Cheng[2,*]
[1]*Department of Electrophysics, National Chiayi University, Chiayi city 60004, Taiwan, Republic of China*
[2]*Department of Optoelectric Physics, Chinese Culture University, Taipei 11114, Taiwan, Republic of China*

(Received 18 April 2018; revised manuscript received 17 July 2018; published 17 September 2018)

A gap soliton is a solitonic state existing inside the band gap of an infinite-periodic exciton-polariton condensate (EPC). The combination of surface states and gap solitons forms the so-called surface gap solitons (SGSs). We analyze the existence of SGSs near the interface between uniform and semi-infinite periodic EPCs. We find that SGSs exist only when the system is excited by a pump with a smaller width. As the width of the pump increases, SGSs become unstable.

DOI: 10.1103/PhysRevE.98.032212

I. INTRODUCTION

Solitons, nonspreading localized waves [1], are created when the nonlinear focusing dynamics compensates the spreading due to dispersions. The bright gap soliton, which is a solitonic state existing inside the band gap of infinite-periodic systems, was observed in periodic photonic [2,3] and matter-wave [4,5] band structures. Solitons in laser cavities based on planar waveguides exhibit two types of solitons: hyperbolic-secant-type and hyperbolic-cosecant-type solitons, when the complex Ginzburg-Landau equation has modified to contain background linear loss and locally applied gain [6]. The dissipative gap solitons in optical cavities with a periodic modulation of the refractive index, self-defocusing nonlinearity, gain, and saturable absorption are also studied using the complex Ginzburg-Landau equation [7]. Stable dissipative gap solitons could exist if the periodic modulation of the refractive index is larger and gain has an intermediate strength.

In recent years, exciton-polariton condensates (EPCs) created in semiconductor microcavities [8] have been the subject of intensive research because of their potential advances towards a new generation of low-threshold lasers and ultrafast optical amplifiers and switches at room temperature [9]. The EPC in a static [10,11] or tunable [12,13] periodic potential has been realized to study the s- and p-type wave functions, which could have different energies, symmetry, and spatial coherence. Understanding the properties of EPCs in a periodic potential is of importance towards developing quantum simulation on which many researchers have been working with cold atoms or ion traps [14]. The solitonic gap states were observed by using a laser pump aimed at the barrier region of the one-dimensional periodic potential [15], which was produced by laterally modulated micrometal wires. The defocusing nonlinearity is balanced by the anomalous dispersion relation in the formation of a bright gap soliton in EPCs [16]. The resonantly excited gap solitons were also observed in a two-dimensional square lattice [17,18]. A mechanism for self-localization of EPCs was theoretically proposed due to effective potentials induced by the exciton-polariton flows [19]. Dark gap solitons were also shown to be possible in EPCs [20]. Nevertheless, the studies of surface solitonic modes, named surface gap solitons (SGSs), in EPCs are scarce nowadays. SGSs are polaritonic waves that combine surface states and gap solitons into nonlinear localized states near the interface between uniform and semi-infinite periodic EPCs. The polaritonic SGSs can be in analogy to the optical nonlinear Tamm states [21–23].

In this paper, the effects of spatial localized SGSs of EPCs are investigated by exciting the system via pumps with various powers and widths. We demonstrate that there are stable SGSs inside the first and second band gaps induced by the periodic potential if the width of the pump profile is smaller.

II. THEORETICAL MODEL AND FORMALISM OF LOCALIZED SGSS IN EPCS

In the theoretical modeling of the EPC, we rely on the mean-field complex Gross-Pitaveskii equation introduced by Keeling and Berlo [24], incorporating the external potential, interparticle interactions, pump, and loss:

$$i\hbar\frac{\partial\Psi}{\partial t} = -\frac{\hbar^2}{2m}\frac{\partial^2\Psi}{\partial x^2} + \tilde{V}(x)\Psi + U|\Psi|^2\Psi + i(\gamma_{\text{eff}} - \Gamma|\Psi|^2)\Psi, \quad (1)$$

where Ψ is the wave function, and $\hbar$ and m are Planck's constant and exciton-polariton mass, respectively. $\tilde{V}(x)$ is a one-dimensional external potential given by $\tilde{V}(x) = \tilde{V}_1\sin^2(\pi x/a)$ and $\tilde{V}(x) = \tilde{V}_2$ if $x \geqslant 0$ and $x < 0$, respectively. Here a is the lattice constant of the periodic potential, and U is the strength of repulsive interactions between exciton-polaritons. γ_{eff} represents the linear net gain describing the balance between the stimulated scattering of exciton-polaritons into the condensate and the linear loss of exciton-polaritons out of the cavity. Γ is the coefficient of gain saturation.

Let the timescale be $1/\omega$, where $\omega = 4\hbar/ma^2$. Choosing lengths in units of $a/2$, energies in units of $\hbar\omega$, and the wave

*scheng@faculty.pccu.edu.tw

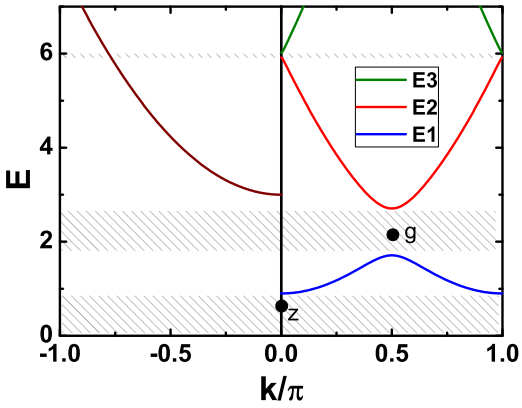

FIG. 1. Energy dispersion relations without pump and loss effects for $V_1 = 2$ and $V_2 = 3$. Energies of $E_1(k = 0)$, $E_1(k = \pi/2)$, and $E_2(k = \pi/2)$ are 0.900, 1.710, and 2.707, respectively.

function $\Psi \to \sqrt{\hbar\omega/U}\Psi$ with respect to U, the steady states of Eq. (1) are obtained by taking the wave function $\Psi(x,t) = \psi(x)e^{-iEt}$, where E is the chemical potential or excitation energy of the system. Then Eq. (1) becomes

$$\frac{1}{2}\frac{\partial^2\psi}{\partial x^2} + [E - V(x)]\psi - |\psi|^2\psi - i[\alpha(x) - \sigma|\psi|^2]\psi = 0, \tag{2}$$

where $\sigma = \Gamma/U$. The external potential $V(x)$ is given by $V(x) = V_1 \sin^2(\pi x/2)$ and $V(x) = V_2$ in the regions $x \geqslant 0$ and $x < 0$, respectively, where $V_1 = \tilde{V}_1/\hbar\omega$ and $V_2 = \tilde{V}_2/\hbar\omega$. Polaritons are affected by the uniform and periodic external potentials on the left-hand side and right-hand side of the one-dimensional system, respectively. Hence, the energy dispersion relations in Fig. 1 show a parabolic relation for $x < 0$ and multiple band structures for $x \geqslant 0$. The existence of the periodic potential splits the energy dispersion of the positive wave vector into multiple bands with the band edge occurring at $k = \pi/2$ (see Fig. 1). The lowest and intermediate energy bands labeled $E_1(k)$ and $E_2(k)$ are the first and second bands, respectively. The lowest and first band gap is located below the first band center at $k = 0$. The second band gap lies above the first band edge at $k = \pi/2$. In this paper $\sigma = 0.52$ is chosen so that the first-band width in Fig. 1 is 1 meV, shown in Ref. [10]. We consider the pump with a finite width, i.e., $\alpha(x) = \alpha_0 e^{-(x/w)^2}$ with pump parameter $\alpha_0 = \gamma_{\text{eff}}/\hbar\omega$ and width w.

Before solving Eq. (2) to find the steady states of SGSs, we would like to obtain the linear band structure of an infinite periodic potential and its corresponding Bloch states. Due to the external potential being composed of uniform and semiperiodic potentials, the wave function $\psi(x)$ is then divided into two parts: $\psi(x) = \psi_<(x)$ and $\psi(x) = \psi_>(x)$ in the regions $x < 0$ and $x \geqslant 0$, respectively. Ignoring the nonlinear, loss, and pump effects, the Bloch wave function $\chi(x)$ is given by the form $\chi_{n,k}(x) = e^{ikx}u_{n,k}(x)$, where k is the quasimomentum and n indicates the band index. The Bloch functions $u_{n,k}(x)$ are periodic with period 2, i.e., $u_{n,k}(x + 2) = u_{n,k}(x)$. In this case, the function $u_{n,k}(x)$ is expanded by a Fourier series in the reciprocal momentum space, i.e., $u_{n,k}(x) = \sum_m C_m^n e^{imGx}$, where C_m^n are the expansion coefficients of the Bloch function and $G = \pi$ is the reciprocal wave vector. Therefore, the linear spectra of an EPC consist of bands of eigenenergies $E_n(k)$.

After finding the Bloch bands and their corresponding wave functions, we apply the effective-mass approximation [20,25,26] to Eq. (2). The nonlinear and nonequilibrium effects are treated as the perturbations. A wave packet $\psi_>(x)$ with a momentum distribution centered around $k_0 = \pi/2$ at the $n = 1$ band edge is described by a slowly varying envelope $F(x)$ (on the scale of several lattice constants) multiplied by the Bloch wave function as $\psi_>(x) = F(x)\chi_{1,k_0}(x)$. In the case of weakly interacting polaritons and negligible band mixing, the steady-state envelop $F(x)$, with energy E near the band edge at k_0, satisfies the time-independent differential equation written as

$$\frac{1}{2m^*(x)}\frac{d^2F(x)}{dx^2} + \delta F(x) - \lambda|F(x)|^2F(x) - i[\alpha(x) - \sigma\lambda|F(x)|^2]F(x) = 0, \tag{3}$$

where $1/m^* = \frac{d^2E_1(k)}{dk^2}|_{k=k_0}$ is the inverse effective mass of the exciton-polariton. $\delta = E - E_1(k_0)$ is the detuning energy above the band edge of the first band. Due to the periodicity, the interaction strength between exciton-polaritons is renormalized by a factor λ, where $\lambda = \int_{-1}^{1}|\chi_{1,k_0}(x)|^4\,dx/\int_{-1}^{1}|\chi_{1,k_0}(x)|^2\,dx$. The periodic potential determines the energy bands and effective masses through the formalism of Bloch wave functions. It also leads to a group velocity v_g of the wave packet determined by the energy band via $v_g(k_0) = \frac{dE_1(k)}{dk}|_{k=k_0}$. We have $v_g(k_0) = 0$ at $k_0 = 0$ and $k = \pi/2$. In EPCs with a negative effective mass, a bright soliton can be achieved due to the repulsive nonlinearity in EPCs being reversed into an attractive nonlinearity that can then balance the dispersion effect [17,18].

Equation (3) determines the envelope of the steady wave function $\psi_>(x)$ in the region of $x \geqslant 0$. The steady wave function $\psi_<(x)$ in the region of $x < 0$ is determined by Eq. (2) with $V(x) = V_2$. Still, there are no simple analytic solutions of Eqs. (2) and (3). We have to rely on the Newton-Ralphson method (NRM) to solve both equations numerically. Applying the NRM, we need an initial wave function to generate a self-consistent solution of a SGS. A toy-model equation [20] and its analytic solution, $\phi(x)$, could be obtained if $|\psi_<(x)|^2$ in Eq. (2) and $|F(x)|^2$ in Eq. (3) are replaced by $\psi_<(x)^2$ and $F(x)^2$, respectively. We then use $\phi(x)$ as the initial wave function of the NRM to solve Eqs. (2) and (3) consistently. The wave function $\phi(x)$ of the toy model is determined by

$$\frac{1}{2M(x)}\frac{d^2\phi(x)}{dx^2} + \Delta(x)\phi(x) - \Lambda(x)\phi(x)^3 - i[\alpha(x) - \sigma\Lambda(x)\phi(x)^2]\phi(x) = 0, \tag{4}$$

where $M(x) = m^*$, $\phi_>(x) = F(x)$, $\Delta(x) = \delta$, and $\Lambda(x) = \lambda$ in the region $x \geqslant 0$. In the region $x < 0$, $M(x) = 1$, $\phi_<(x) = \psi_<(x)$, $\Delta(x) = \epsilon$, and $\Lambda(x) = 1$, where $\epsilon = E - V_2$.

We could find the analytic solution of Eq. (4) if the pump profile $\alpha(x)$ is treated as a uniform pump with pump parameter α_0, i.e., $\alpha(x) = \alpha_0$. In this paper, we take the excitation energy E is lying below the potential energy V_2 and inside the energy gaps labeled by points "g" and

"z" of Fig. 1. Therefore, ϵ is always less than zero. The hyperbolic-cosecant-type and hyperbolic-secant-type SGSs [6] could occur inside the band gaps labeled by the points "z" and "g" in Fig. 1, whose detuning energies δ are less and greater than zero, respectively. Then in the region of $x \geqslant 0$, Eq. (4) with $\delta < 0$ and $\delta > 0$ has a hyperbolic-cosecant-type solution $\phi_>(x) = C_1\mathrm{csch}(B_1x + \theta_1)$ and hyperbolic-secant-type solution $\phi_>(x) = C_2\mathrm{sech}(B_2x + \theta_1)$, respectively. There is also a solution of $\phi_<(x) = C_3\mathrm{csch}(B_3x + \theta_2)$ in the region $x < 0$. Here $B_1 = \sqrt{2m^*(|\delta| + i\alpha_0)}$, $C_1 = \sqrt{2(|\delta| + i\alpha_0)/[\lambda(1 - i\sigma)]}$, $B_2 = \sqrt{2|m^*|(\delta - i\alpha_0)}$, $C_2 = \sqrt{2(\delta - i\alpha_0)/[\lambda(1 - i\sigma)]}$, $B_3 = \sqrt{2(|\epsilon| + i\alpha_0)}$, and $C_3 = \sqrt{2(|\epsilon| + i\alpha_0)/(1 - i\sigma)}$. The phases θ_1 and θ_2 are determined by the boundary conditions that $\phi_>(x)|_{x=0} = \phi_<(x)|_{x=0}$ and $\frac{d\phi_>(x)}{dx}|_{x=0} = \frac{d\phi_<(x)}{dx}|_{x=0}$, where $\phi_>(x) = \phi_>(x)\chi_{1,k_0}(x)$. The analytical hyperbolic solutions provides qualitative understanding that the SGS is self-localized near the interface between uniform and semi-infinite periodic potentials.

III. STEADY-STATE PROFILES OF THE SGSS

After finding the analytic solution of Eq. (4), wave functions $\phi_>(x)$ and $\phi_<(x)$ are treated as the initial wave function $\psi(x)$ in the NRM of solving Eq. (2) to obtain a SGS numerically. The self-consistent solutions of hyperbolic-secant-type SGSs and hyperbolic-cosecant-type SGSs are shown in Figs. 2(a) and 2(b) and Fig. 2(c) and 2(d), respectively. With the disperse effect being balanced by the attractive nonlinearity, a hyperbolic-secant-type SGS is achieved inside the second band gap. No hyperbolic-cosecant-type SGS exists inside the second band gap. But a hyperbolic-cosecant-type SGS can occur inside the first band gap due to the defect effect created by the discontinuity at the surface of the external potential. The SGS density distributions for two different V_1 values are shown by red solid curves. The density distributions monotonically diminish from the interface between uniform and semi-infinite periodic potentials towards the left-hand and right-hand sides. Due to $E < V_2$, the uniform potential on the left-hand side of the interface creates a barrier to prevent the SGS from delocalizing. Still, there are some exciton-polaritons penetrating the barrier and accumulating near the left-hand side of the interface.

On increasing the pump parameter from $\alpha_0 = 0.5$ to $\alpha_0 = 1.5$ as shown in Fig. 3, the peak amplitude $(|\psi(x)|)_{\mathrm{peak}}$ (or the peak density) from accumulated exciton-polaritons is growing higher, and its position (x_{peak}) shifts towards the interface. The dependence of $(|\psi(x)|)_{\mathrm{peak}}$ and x_{peak} on the pump parameter is shown in Fig. 4. On the right-hand side of the interface, the hyperbolic-secant-type SGS density displays an oscillating and gradually diminishing distribution. The crests of the oscillating density are centered on the periodic potential minima due to the expulsive force from the potential. For a hyperbolic-cosecant-type SGS, the density is well localized at the interface, and the oscillating density into the right-hand periodic potential is not obvious. The band gap from the periodic potential forbids the EPC to propagate toward the right-hand side if $\delta > 0$. The density profiles of SGSs would change if the periodic potential depth is higher than the uniform potential depth, i.e., $V_1 > V_2$ shown in Figs. 2(b) and 2(d) and 3(b) and 3(d). The peak amplitude of the SGS tilts towards the

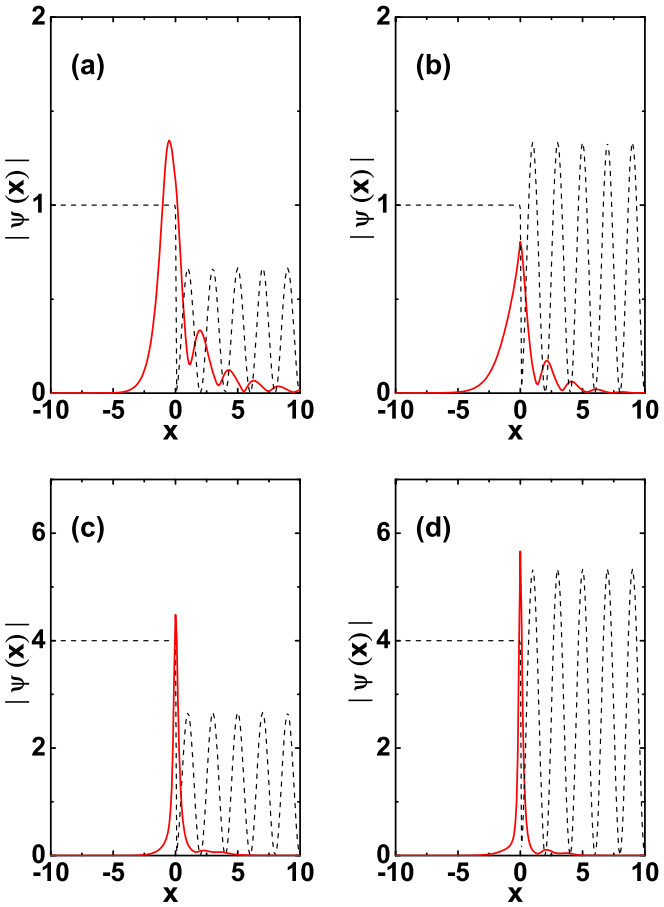

FIG. 2. Density profiles of surface gap solitons with $V_2 = 3$, $\alpha_0 = 0.5$, and $w = 0.5$. (red solid curves): (a) a hyperbolic-secant-type SGS with $V_1 = 2$ and $E = 2.110$, (b) a hyperbolic-secant-type SGS with $V_1 = 4$ and $E = 2.542$, (c) a hyperbolic-cosecant-type SGS with $V_1 = 2$ and $E = 0.700$, (d) a hyperbolic-cosecant-type SGS with $V_1 = 4$ and $E = 1.420$. The black dashed curve is the relative strength of the external potential.

interface. The maxima density is reducing and increasing for a hyperbolic-secant-type SGS and hyperbolic-cosecant-type SGS, respectively, as V_1 gets larger. The number of crests of the oscillating density of a hyperbolic-secant-type SGS is also decreasing.

IV. BOGOLIUBOV EXCITATIONS AND STABILITIES OF THE SGSS IN EPC

Bogoliubov excitations can be studied by inserting into rescaled Eq. (1) a solution that has small perturbations to the steady wave function [27]. Then $\Psi(x,t) = e^{-iEt}[\psi(x) + u_q(x)e^{iqx}e^{-i\Omega t} - v_q^*(x)e^{-iqx}e^{i\Omega t}]$, where $u_q(x)$ and $v_q(x)$ are the amplitudes of Bogoliubov quasiparticles with wave vector q. Substituting $\Psi(x,t)$ into the time-dependent equation of Eq. (2), we can obtain two coupled Bogoliubov equations to realize the stability of the SGSs through the complex-valued Ω. Then Eq. (4) becomes a non-Hermitian matrix eigenvalue problem:

$$\begin{pmatrix} L_+ & -\phi^2(x)(1 - i\sigma) \\ \phi^{*2}(x)(1 + i\sigma) & L_- \end{pmatrix}\begin{pmatrix} u_q \\ v_q \end{pmatrix} = \Omega\begin{pmatrix} u_q \\ v_q \end{pmatrix}, \tag{5}$$

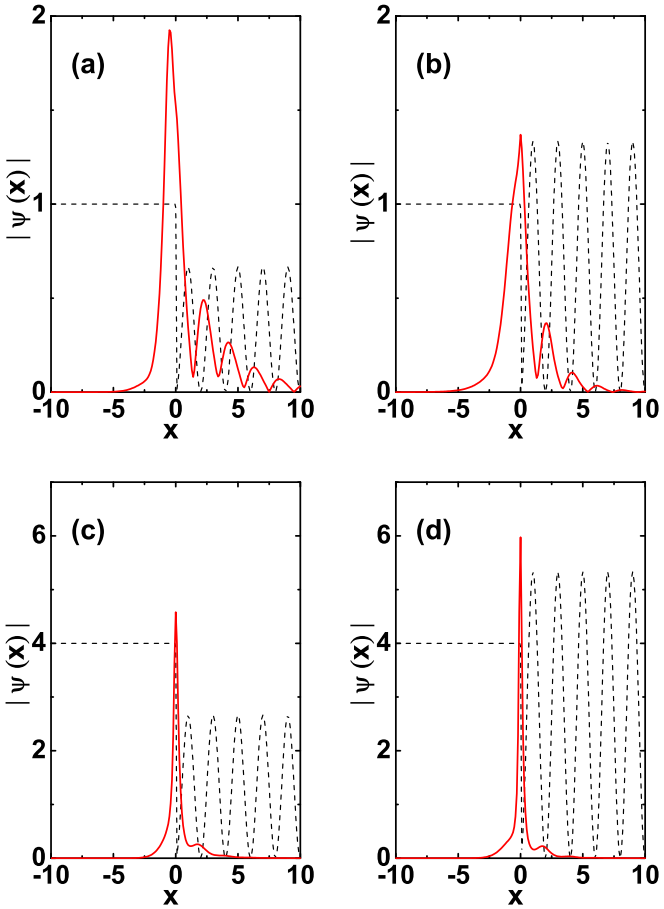

FIG. 3. Density profiles of surface gap solitons with $V_2 = 3$, $\alpha_0 = 1.5$, and $w = 0.5$. (red solid curves): (a) a hyperbolic-secant-type SGS with $V_1 = 2$ and $E = 2.110$, (b) a hyperbolic-secant-type SGS with $V_1 = 4$ and $E = 2.542$, (c) a hyperbolic-cosecant-type SGS with $V_1 = 2$ and $E = 0.700$, (d) a hyperbolic-cosecant-type SGS with $V_1 = 4$ and $E = 1.420$. The black dashed curve is the relative strength of the external potential.

where $L_\pm = \mp\frac{1}{2}\frac{d^2}{dx^2} \pm V(x) \pm 2|\phi(x)|^2 + i\alpha - 2i\sigma|\phi(x)|^2 \mp E$. If the system has one eigenvalue with a positive imaginary part, the corresponding mode will grow exponentially in time. The system is then dynamically unstable and might evolve into gap solitons. The stability limit is obtained from the condition that the imaginary part of the eigenvalue is greater than zero.

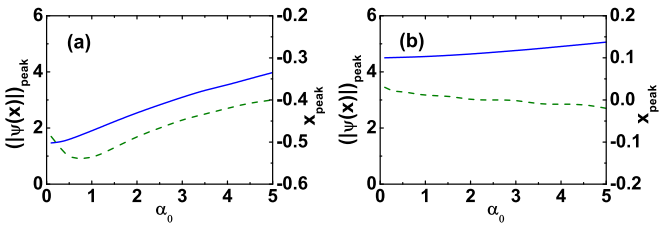

FIG. 4. Peak amplitude $[(|\psi(x)|)_{\text{peak}}$, solid line] and position (x_{peak}, dashed line) of SGSs with $V_1 = 2$ and $V_2 = 3$. (a) A hyperbolic-secant-type SGS with $\delta = 0.4$ and $w = 0.3$; (b) a hyperbolic-cosecant-type SGS with $\delta = -0.2$ and $w = 0.5$.

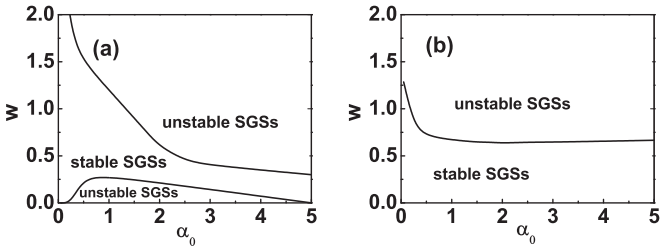

FIG. 5. Phase boundaries between stable and unstable SGSs with $V_1 = 2$ and $V_2 = 3$. (a) A hyperbolic-secant-type SGS with $\delta = 0.4$ and $E = 2.110$; (b) a hyperbolic-cosecant-type SGS with $\delta = -0.2$ and $E = 0.700$.

For various pump powers and widths, the phase boundaries between stable and unstable hyperbolic-secant-type SGSs in the second band gap (lying between the first and second bands) and hyperbolic-cosecant-type SGSs in the first band gap (lying below the first band) are shown in Figs. 5(a) and 5(b), respectively. The SGSs become unstable in regimes with higher pump powers and larger pump widths or with very narrow pumps. A hyperbolic-secant-type SGS is stable if the gain is smaller and this behavior is different from the dissipative gap solitons in optical cavities. A dissipative gap soliton becomes unstable if the gain is larger or smaller [7]. For a large pump width, a SGS owns a much broad density distribution which can be easily delocalized away from the interface. Therefore, a SGS under a uniform pump is unstable. A SGS under a very narrow pump does not have enough density to balance the dispersion effect and therefore becomes unstable. In a given pump power, stable hyperbolic-secant-type SGSs exist when the pump owns an intermediate width. On the right-hand side of the interface, the number of density sidelobes of a stable SGS is unaffected by the pump power. On the other hand, the width of the highest density peak decreases as the pump power increases. Also, the stable region of the hyperbolic-cosecant-type SGS exists for a smaller pump width and does not change with respect to the pump power. However, for a given pump power, hyperbolic-cosecant-type SGSs can exist even the pump width is very small.

While fixing $\alpha_0 = 1$ and $V_2 = 3$, two new phase boundaries are drawn in Fig. 6. One is the border, shown by the blue dashed curve, for V_1 versus w. Another is the border,

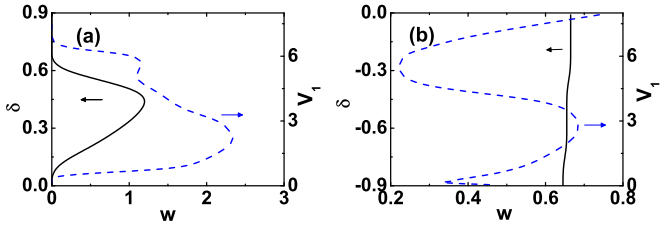

FIG. 6. The numerically identified stable regions for SGSs are located on the left-hand side of borders, which are shown for $\alpha_0 = 1$ and $V_2 = 3$. (a) Hyperbolic-secant-type SGSs: The black solid curve is the borders of δ versus w with $V_1 = 2$. The blue dashed curve is the border of V_1 versus w with $\delta = 0.4$. (b) Hyperbolic-cosecant-type SGSs : The black solid curve is the borders of δ versus w with $V_1 = 2$. The blue dashed curve is the border of V_1 versus w with $\delta = -0.2$.

shown by the black solid curve with $V_1 = 2$, for δ versus w. Stable phases are on the left hand of curves. From the blue dashed line, we conclude that a shallow semiperiodic potential does not create a large enough band-gap to localize a hyperbolic-secant-type SGS. This conclusion is consistent with the previous study of the dissipative gap solitons [7]. Stable dissipative gap solitons could exist if the periodic modulation of the refractive index is larger [7]. There is also no localized hyperbolic-secant-type SGS in a deeper semiperiodic potential, which produces a band-edge energy higher than the uniform potential barrier, i.e., $\epsilon > 0$. Near the first band edge with a smaller energy detuning inside the gap, a hyperbolic-secant-type SGS owns a much broad density distribution and is easily delocalized away from the interface [see the black solid line in Fig. 4(a)]. On the other hand, shifting the detuning close to the second band edge, the nonlinearity of an EPC gradually changes from the attractive nonlinearity into the repulsive nonlinearity. No stable hyperbolic-secant-type SGS with repulsive nonlinearity can exist in EPCs. The same investigation done on hyperbolic-cosecant-type SGSs [see Fig. 6(b)] reveals that they are unstable as the periodic potential depth owns an intermediate depth. The border for δ versus w in Fig. 6(b) is not significantly affected by the change of the detuning energy.

In Ref. [28] the dissipative surface solitons forming at the interface between a semi-infinite lattice and a homogeneous Kerr medium was reported. When a gain is applied at the interface between a homogeneous and a periodic medium, the dissipative surface solitons can be pinned by the defect channel realized by the gain. In our case here, the polariton-polariton repulsive interaction resembles to a defocusing media. Figure 3(a) in Ref. [28] is not applicable in polariton system. In comparison to Fig. 3(b) in Ref. [28], we obtain the existence domain with respect to pump parameter and coefficient of nonlinear losses shown in Fig. 7. In Ref. [28] the surface solitons exist between a lower and upper values of gain coefficient. However, in Fig. 7 the result of the existence domain is different. The difference should be from the finite pump spot in our polariton system, and we assume a Gaussian pump profile $\alpha(x) = \alpha_0 e^{-(x/w)^2}$ rather than a periodic $\alpha(x) = \alpha_0 \sin^2(2x)$. Moreover, the existence domains of the hyperbolic-secant-type and hyperbolic-cosecant-type SGSs are different. For the hyperbolic-cosecant-type SGS with pump width $w = 0.5$ and a given coefficient of nonlinear losses σ, the gap soliton is stable when the pump parameter is below a threshold value. But for hyperbolic-secant-type SGS with pump width $w = 0.5$, in particular $0.1 < \sigma < 0.4$, the gap soliton is stable when the pump parameter exceeds a threshold value, and there also exists the upper bound for the allowed pump parameter at which the gap solitons can still be found.

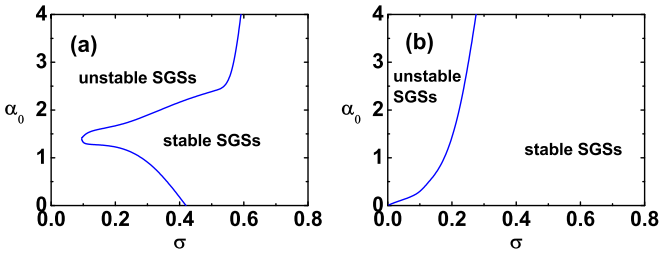

FIG. 7. The numerically identified stable regions for SGSs are located on the right-hand side of borders, which are shown for $V_1 = 2$, $V_2 = 3$ and $w = 0.5$. (a) Hyperbolic-secant-type SGSs with $\delta = 0.4$. (b) Hyperbolic-cosecant-type SGSs with $\delta = -0.2$.

V. CONCLUSIONS

In summary, we showed that stable SGSs could be created near the interface between uniform and semi-infinite periodic EPCs. A defect is created by the discontinuity between uniform and periodic potentials, and periodicity induces a nonlinear character change. There are stable hyperbolic-secant-type SGSs and hyperbolic-cosecant-type SGSs with energies above the band edge with an anomalous dispersion relation and below the band center with a normal dispersion relation on the first band, respectively. The defocusing nonlinearity is balanced by the anomalous dispersion relation in the formation of hyperbolic-secant-type SGSs in EPCs. A stable hyperbolic-cosecant-type SGS is pinned by a defect near the interface between uniform and semi-infinite periodic EPCs. We also reported the dynamical instability of SGSs. We show that SGSs become unstable as the pump power or width is increasing. No stable SGSs exist in a uniformly pumped EPC.

ACKNOWLEDGMENTS

We acknowledge financial support from Ministry of Science and Technology of the Republic of China under Contract No. MOST105-2112-M-034-001-MY3 and MOST105-2112-M-415-009-MY3.

[1] J. S. Russell, Report of the 14th Meeting of the British Association for the Advancement of Science **47–57**, 311 (1845).
[2] Y. S. Kivshar, Opt. Lett. **20**, 1147 (1993).
[3] J. Feng, Opt. Lett. **20**, 1302 (1993).
[4] B. Eiermann, P. Treutlein, T. Anker, M. Albiez, M. Taglieber, K. P. Marzlin, and M. K. Oberthaler, Phys. Rev. Lett. **91**, 060402 (2003).
[5] B. Eiermann, T. Anker, M. Albiez, M. Taglieber, P. Treutlein, K. P. Marzlin, and M. K. Oberthaler, Phys. Rev. Lett. **92**, 230401 (2004).
[6] C.-K. Lam, B. A. Malomed, K. W. Chow, and P. K. A. Wai, Eur. Phys. J. Special Topics **173**, 233 (2009).
[7] H. Sakaguchi and B. A. Malomed, Phys. Rev. E **77**, 056606 (2008).
[8] J. Kasprzak, M. Richard, S. Kundermann, A. Baas, P. Jeambrun, J. M. J. Keeling, F. M. Marchetti, M. H. Szymańska, R. André, J. L. Staehli *et al.*, Nature (London) **443**, 409 (2006).
[9] H. Deng, H. Haug, and Y. Yamamoto, Rev. Mod. Phys. **82**, 1489 (2010).

[10] C. W. Lai, N. Y. Kim, S. Utsunomiya, G. Roumpos, H. Deng, M. D. Fraser, Y. Byrnes, P. Recher, N. Kumada, T. Fujisawa *et al.*, Nature (London) **450**, 529 (2007).
[11] N. Y. Kim, K. Kusudo, C. Wu, N. Masumoto, A. Löffler, S. Höfling, N. Kumada, L. Worschech, A. Forchel, and Y. Yamamoto, Nat. Phys. **7**, 681 (2011).
[12] E. A. Cerda-Méndez, D. N. Krizhanovskii, M. Wouters, R. Bradley, K. Biermann, K. Guda, R. Hey, P. V. Santos, D. Sarkar, and M. S. Skolnick, Phys. Rev. Lett. **105**, 116402 (2010).
[13] D. N. Krizhanovskii, E. A. Cerda-Méndez, S. Gavrilov, D. Sarkar, K. Guda, R. Bradley, P. V. Santos, R. Hey, K. Biermann, M. Sich *et al.*, Phys. Rev. B **87**, 155423 (2013).
[14] I. Buluta and F. Nori, Science **326**, 108 (2009).
[15] D. Tanese, H. Flayac, D. Solnyshkov, A. Amo, A. Lemaître, E. Galopin, R. Braive, P. Senellart, I. Sagnes, G. Malpuech *et al.*, Nat. Commun. **4**, 1749 (2013).
[16] O. A. Egorov, D. V. Skryabin, A. V. Yulin, and F. Lederer, Phys. Rev. Lett. **102**, 153904 (2009).
[17] A. V. Gorbach, B. A. Malomed, and D. V. Skryabin, Phys. Lett A. **373**, 3024 (2009).
[18] E. A. Cerda-Méndez, D. Sarkar, D. N. Krizhanovskii, S. S. Gavrilov, K. Biermann, M. S. Skolnick, and P. V. Santos, Phys. Rev. Lett. **111**, 146401 (2013).
[19] E. A. Ostrovskaya, J. Abdullaev, M. D. Fraser, A. S. Desyatnikov, and Y. S. Kivshar, Phys. Rev. Lett. **110**, 170407 (2013).
[20] S. C. Cheng and T. W. Chen, Phys. Rev. E **97**, 032212 (2018).
[21] S. Suntsov, K. G. Makris, D. N. Christodoulides, G. I. Stegeman, A. Haché, R. Morandotti, H. Yang, G. Salamo, and M. Sorel, Phys. Rev. Lett. **96**, 063901 (2006).
[22] Y. V. Kartashov, V. A. Vysloukh, and L. Torner, Phys. Rev. Lett. **96**, 073901 (2006).
[23] C. R. Rosberg, D. N. Neshev, W. Krolikowski, A. Mitchell, R. A. Vicencio, M. I. Molina, and Y. S. Kivshar, Phys. Rev. Lett. **97**, 083901 (2006).
[24] J. Keeling and N. G. Berloff, Phys. Rev. Lett. **100**, 250401 (2008).
[25] V. A. Brazhnyi, V. V. Konotop, and V. M. Pérez-García, Phys. Rev. Lett. **96**, 060403 (2006).
[26] C. M. de Sterke, D. G. Salinas, and J. E. Sipe, Phys. Rev. E **54**, 1969 (1996).
[27] R. Ozeri, N. Katz, J. Steinhauer, and N. Davidson, Rev. Mod. Phys. **77**, 187 (2005).
[28] Y. V. Kartashov, V. V. Konotop, and V. A. Vysloukh, Europhys. Lett. **91**, 34003 (2010).